University Library

MINERVA ACCESS

A gateway to Melbourne's research publications

Minerva Access is the Institutional Repository of The University of Melbourne

Author/s:
Boldt, K;Schwarz, KN;Kirkwood, N;Smith, TA;Mulvaney, P

Title:
Electronic Structure Engineering in ZnSe/CdS Type-II Nanoparticles by Interface Alloying

Date:
2014-06-19

Citation:
Boldt, K., Schwarz, K. N., Kirkwood, N., Smith, T. A. & Mulvaney, P. (2014). Electronic Structure Engineering in ZnSe/CdS Type-II Nanoparticles by Interface Alloying. The Journal of Physical Chemistry C: Energy Conversion and Storage, Optical and Electronic Devices, Interfaces, Nanomaterials, and Hard Matter, 118 (24), pp.13276-13284. https://doi.org/10.1021/jp503609f.

Persistent Link:
https://hdl.handle.net/11343/324783

Electronic Structure Engineering in ZnSe/CdS Type-II Nanoparticles by Interface Alloying

Klaus Boldt,* Kyra N. Schwarz, Nicholas Kirkwood, Trevor A. Smith, and Paul Mulvaney*

School of Chemistry and Bio21 Institute, University of Melbourne, Parkville VIC, 3010, Australia

E-mail: klaus.boldt@unimelb.edu.au; mulvaney@unimelb.edu.au

KEYWORDS: quantum dots, overlap integral, transient absorption spectroscopy, stimulated emission, optical gain, effective mass approximation

*To whom correspondence should be addressed

Abstract

We report the synthesis and characterization of Type-II ZnSe/CdS semiconductor nanocrystals that exhibit strong charge separation, high photoluminescence quantum yields, low optical gain thresholds, and alloyed core-shell interfaces. Shell growth rates and the degree of alloying both depend strongly on the shelling temperature. The core-shell NCs exhibit band edge PL with emission wavelengths spanning the blue to orange region of the electromagnetic spectrum (380-562 nm). Fluorescence quantum yields up to 75 % can be obtained by deposition of an additional ZnS layer. Transient absorption spectroscopy reveals that the population of the first two exciton states ($1S_e$-$1S_h$, $1S_e$-$2S_h$) in the Type II structures can be controlled by alloying. Increased alloying leads to greater population of the 2S hole state exciton.

INTRODUCTION

Core/shell structures have been used extensively to control the electronic structure of semiconductor nanocrystals or quantum dots (QDs).[1–4] Three different structures are commonly recognized: In a type-I structure, the charge carriers are confined to the particle core by the large band offsets of both the conduction and valence bands of the shell material. Conversely, in a type-II structure there is separation of excited electrons and holes into either the core or shell by a staggered band structure, leading to extended exciton lifetimes and luminescence emission energies below what is achievable with either the core or shell material alone. The intermediate case, in which one charge carrier is localized to the core and the other is delocalized over the whole structure is known as type-I$^{1/2}$ or *quasi*-type-II.[5]

In contrast to type-I structures, which are now routinely prepared with photoluminescence quantum yields (PL QY) close to unity,[6] type-II particles have long suffered from comparatively weak luminescence and low chemical- and photo-stability.[7,8] These problems are to some extent intrinsic to type-II structures: Charge carrier localization into two different regions of a particle decreases the overlap of their wavefunctions and thereby the probability for radiative recombination. Furthermore, one of the charge carrier wavefunctions is strongly localized near the surface,

facilitating extraction by a scavenger, opening additional non-radiative relaxation pathways, and enhancing the rates of photocorrosion.

A high PL QY for type-II particles is of major interest, because these systems possess extremely large, internal dipole moments in the excited state. These cause a Stark-shift of the biexciton absorption to higher energies. If absorption of a second photon is sufficiently blue-shifted above the ensemble line width, generation of single excitons does not result in optical transparency at the exciton ground state energy nor does it lead to Auger excitation of the excited charge carriers, and gain is expected to occur at excitation levels below an average excited nano crystal (NC) population of $\langle N \rangle = 1$. This makes these particles ideal contestants for lasing in the single exciton regime.[9,10] In recent years progress has been made towards increasing the luminescence of type-II particles through improved preparative routes[11,12] and by growing additional shells that separate both charge carriers from the particle surface in a "type-II in type-I" core/shell/shell structure.[13]

Bulk ZnSe and CdS have a calculated conduction band offset of 0.63 eV, which is larger than that of CdSe/CdTe (0.27 eV), another often-used combination for the fabrication of type-II QDs. Theoretical and experimental values of the valence band offsets for ZnSe/CdS and CdSe/CdTe vary, but tend to have a slightly smaller value for ZnSe/CdS (0.35 eV) than CdSe/CdTe (0.59 eV).[14–19] Considering the higher effective mass of the electron compared to the hole, one can expect efficient charge carrier separation in the ZnSe/CdS heterostructure.

Here we describe the synthesis of highly luminescent ZnSe/CdS type-II nanoparticles with temperature-dependent interface alloying, based on a recent study by Chen et al.[20] and our own work.[21] The alloyed interface was shown to reduce Auger recombination that competes with exciton and biexciton emission.[22] As Kaniyankandy et al. have demonstrated recently for CdSe/CdTe particles, a gradient alloy between core and shell enhances both PL QY and charge separation *via* reduced lattice mismatch and formation of a "separating funnel" for the charges along the gradient.[23] Their layer-by-layer approach of adding mixed Se and Te precursors yielded particles with an alloyed interface, which exhibited twice the fluorescence quantum yield compared to similar particles with sharp core/shell interfaces. However, the ensemble PL QY was overall quite low

($< 1\%$) due to synthesis in aqueous solution.

EXPERIMENTAL METHODS

Chemicals

Cadmium oxide, cadmium acetate, zinc acetate, diethyl zinc in heptane (1 M), *n*- octadecene, oleic acid, oleylamine, tri-*n*-octylphosphine, octane thiol, and selenium were purchased from Sigma-Aldrich. All chemicals and solvents were used as received without further purification.

ZnSe Particle Synthesis

Zinc selenide nanoparticles were prepared following a modified protocol by Cozzoli et al.[24] A Zn/Se prcursor solution was prepared by mixing 1.34 ml of a 1.7 M solution of selenium in TOP, 5.57 ml TOP, and 2.30 ml of a 1 M solution of diethyl zinc in heptane. 8.61 ml oleylamine were loaded into a 25 ml three neck flask equipped with a thermocouple, septum, and condenser inside a nitrogen glove box and heated to 300 °C. A piece of glass wool was used to loosely block the top of the condenser. When the injection temperature was reached 3.21 ml of the injection solution was swiftly injected, and the temperature was immediately adjusted to 265 °C. The particles were allowed to grow for 30 min. 1 ml aliquots of the injection solution were added drop-wise over the course of 5 min every 30 min until the desired particle size was reached.

The reaction mixture was cooled down to room temperature and flocculated with anhydrous ethanol. After centrifuging the sealed vials at 3000 rcf and removing the supernatant the particles were redispersed in anhydrous chloroform. Washing was repeated twice and the particles in chloroform were stored inside a nitrogen glove box until further use. ZnSe particle concentration was approximated from a complete turnover of precursors and corrected by TEM data before and after shell deposition.

CdS Particle Synthesis

Cadmium sulfide particles were prepared following the method by Cao et al.[25] 51.2 mg CdO, 1.0 g oleic acid, and 12 g ODE were loaded into a 50 ml three neck flask and degassed for 1 h at 120 °C under vacuum. The reaction mixture was then placed under nitrogen and heated to 260 °C. 2 ml of a 0.1 M solution of sulfur in ODE were swiftly injected into the solution, and the temperature was set to 240 °C. After 15 min growth was stopped by removing the heat source and cooling to room temperature.

The particles were extracted twice in a separating funnel with a mixture of chloroform and methanol, precipitated from the chloroform phase with acetone, and stored in chloroform. The QD concentration was determined by published methods.[26]

ZnSe/CdS Particle Synthesis

CdS shell deposition on ZnSe nanocrystals was adapted from Chen et al.[20] and our previous work.[21] A cadmium oleate stock solution was prepared by heating 9.6 g (12 ml) of ODE, 0.6 g of cadmium acetate, and 1.47 g (1.65 ml, 2 equiv) oleic acid to 300 °C inside a nitrogen glove box. The heat source was removed when the solution turned clear, and 1.39 g (1.71 ml, 2 equiv) of oleylamine was added to prevent gelling of the solution. The final solution was diluted with ODE as desired.

3 ml of ODE and 3 ml of oleylamine were degassed at 50 °C for 30 min under vacuum. 100 nmol of ZnSe particles in chloroform were then added, and the solvent was removed under vacuum for 15 min at 50 °C and 15 min at 115 °C. The temperature was raised to the chosen reaction temperature (260-310 °C), and starting at 230 °C precursor solutions of cadmium oleate and octane thiol in ODE (3 ml) were added drop-wise with a syringe pump from separate syringes. The amount of Cd was calculated to yield the desired amount of CdS monolayers, and a 1.2-fold excess of thiol was used. After the precursor addition was completed the temperature was adjusted to 200 °C and 1 ml oleic acid was slowly added. The reaction mixture was allowed to stir for 1 h before cooling to room temperature.

The particles were washed three times by flocculating with acetone, centrifuging, and redispersing in chloroform. The final product was passed through a syringe filter and stored under ambient conditions, where it was stable for months.

CdS/ZnSe Particle Synthesis

CdS/ZnSe core/shell particles were prepared following the protocol by Ivanov et al.[11] Briefly, 120 nmol CdS particles in chloroform were mixed with 1.83 ml oleylamine and 6 ml ODE. Volatiles were removed under vacuum at 120 °C for 1 h. The mixture was then heated to 230 °C under a nitrogen atmosphere. The Zn/Se precursor solution was prepared by mixing 110 mg zinc acetate dihydrate, 141 mg oleic acid, and 5 ml TOP. The solution was sonicated until clear, before 0.5 ml (1 equiv) of a 1 M TOPSe solution was added. The precursor solution was added drop-wise to the reaction mixture at a rate of 8 ml/h. After all was added the temperature was lowered to 160 °C and kept overnight. The particles were washed analogously to CdS particles.

ZnS Shell Synthesis

100 nmol of either ZnSe/CdS or CdS/ZnSe particles were placed in a mixture of 3 ml ODE and 3 ml oleylamine and degassed for 1 h at 50 °C and then 15 min at 115 °C. In the case of ZnSe/CdS particles the ZnS shell was usually grown directly after the CdS shell in a one-pot synthesis. The procedure used was analogous to the CdS deposition. The zinc oleate stock solution was prepared with a 0.2 M concentration, and a 2-fold excess of octane thiol was used during addition.[21]

Characterization

TEM measurements were performed with a Tecnai TF20 high-resolution transmission electron microscope with 200 kV accelerating voltage.

Absorption spectroscopy was performed on an Agilent 8453 UV/vis spectrometer. PL spectra and TCSPC was collected in hexane on a Horiba/Jobin Yvon Fluorolog-3 spectrophotometer, using

a 403 nm pulsed diode laser for the fluorescence decay traces. The PL decay curves were fit to a stretched exponential function.

$$I(t) = I_0 \cdot \mathrm{e}^{-(t/\tau)^{\beta}} \tag{1}$$

The lifetime was calculated from the decay signal using:[27]

$$\langle \tau \rangle = \frac{\tau}{\beta} \Gamma \left(\frac{1}{\beta} \right) \tag{2}$$

Nanosecond transient absorption spectra were acquired on an Edinburgh Instruments LP920 spectrometer equipped with an Andor DH720 ICCD camera. Samples were excited using the 355 nm harmonic of a Q-switched Nd:YAG laser (OPOTek Vibrant HE 355 II, pulse width 10 ns, average pulse energy 38.1 mJ). The samples were diluted to an optical density of 0.3 at the excitation wavelength. Each spectrum is the average of 30 measurements, each taken 10 ns after the laser pulse and corrected for laser-induced sample fluorescence. Under these excitation conditions approximately 0.75 excitons were formed per nanoparticle. Nanosecond TA spectra were smoothed using the Savitzky-Golay algorithm of OriginPro 8.6, baseline-corrected, and fitted to two Gaussian functions to extract the relative bleach intensities.

Femto- to picosecond pump-probe transient absorption (TA) spectroscopy was performed using a Ti:sapphire mode-locked oscillator (Coherent, Mira Seed) which seeded a Ti:sapphire regenerative amplifier system (Coherent, RegA 9050) to produce pulses of $\approx$50 fs duration with a repetition rate of 92 kHz with a wavelength centered at 800 nm. A portion of the light was used to generate the 400 nm pump beam using a BBO (barium borate) crystal. The pump beam was mechanically chopped at 4.6 kHz and its position in time relative to the probe was manipulated using a variable optical delay line (Newport, UTS150PP with ESP 300 controller). The visible broadband probe with a range of approximately 440-760 nm was derived from the residual 800 nm beam focused onto a 3 mm sapphire crystal (Crystal Systems). After passing through the sample, the probe beam was analyzed with a CMOS detector (Ultrafast Systems) at 9200 spectra/sec. The pump beam (80 nJ per pulse) had its polarization orientated at 54.7° with respect to the probe. All spectra were

corrected for the chirp of the supercontinuum probe. Further details are available elsewhere.[28]

To measure amplified stimulated emission particles were drop-cast onto a glass coverslip and excited with a Q-switched Nd:YAG laser at 532 nm at 10 Hz close to the band edge transition. The emission was coupled into an optical fibre and detected with an OceanOptics Maya2000 Pro spectrophotometer.

RESULTS AND DISCUSSION

We have prepared ZnSe/CdS by slow addition of cadmium oleate and octane thiol to ZnSe particles in a 1:1 mixture of 1-octadecene and oleylamine under nitrogen on a Schlenk line. The reaction temperature was varied between 260 and 310 °C, and the precursors were added over the course of 1 h, unless otherwise stated. The ZnSe absorption spectrum shows a sharp 1S exciton transition at 375 nm, which shifts rapidly towards lower energies upon addition of Cd and S precursors with a total red-shift of 161 nm at the end of the experiment (Fig. 1A), about twice the shift observed for CdSe/CdS *quasi*-type-II particles.[29,30] With further CdS addition an even larger red-shift was possible, with the largest observed red-shift being 182 nm. During shell growth the band gap transition broadens to a weak shoulder in accordance with the expected decrease of oscillator strength caused by a smaller overlap of the electron and hole wavefunctions. Repeating the reaction at lower temperatures resulted in a comparable shift of the 1S transition, although the peak appeared slightly more defined (see supporting information, Fig. S1). When the precursor injection time was increased from 1 to 2 h at 290 °C, the particles exhibited a 10 nm smaller red-shift (530 nm *vs.* 540 nm). PL lifetimes for the samples prepared at the two addition rates are the same within experimental error when fitted to a stretched exponential function, but the exponent β takes larger values for the slower addition rate, which corresponds to a broader distribution of lifetimes in the sample ($\beta = 1$ being the limit for a monoexponential decay).

The PL spectra had a Gaussian profile with a Stokes shift of 32 nm from the band edge absorption peak. When drop-cast onto a glass coverslip and excited at room temperature with a pulsed

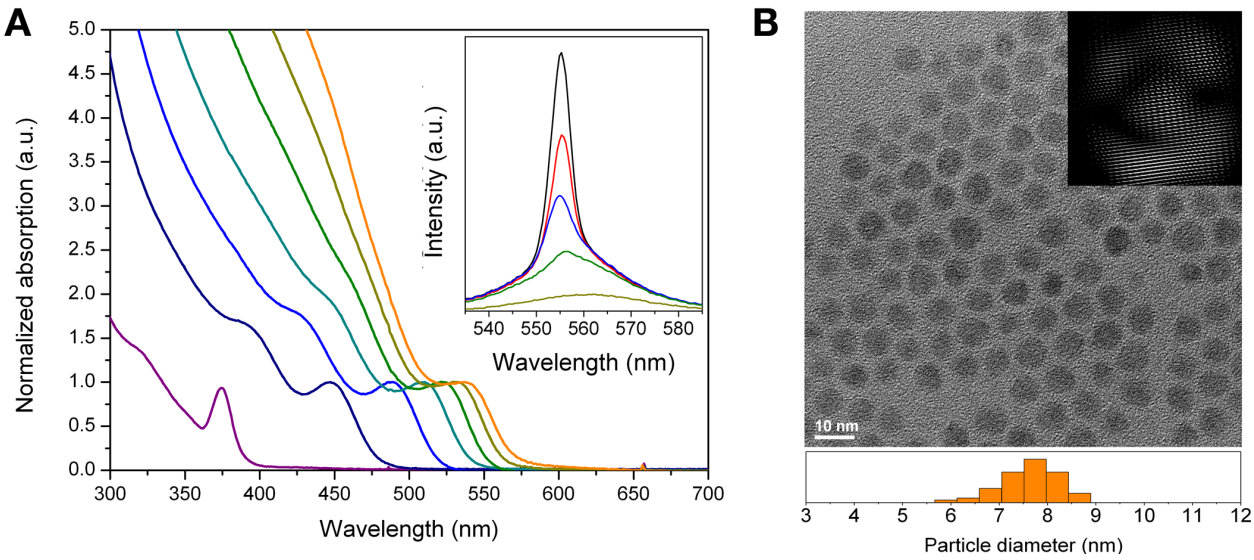


Figure 1: (A) Absorption spectra taken during the growth of 7 ML CdS on 3.6 nm sized ZnSe particles at 310 °C, with samples taken before addition and then every 10 min. The inset shows stimulated emission of closely packed NCs of a comparable sample with pump fluences between 2 and 22 mJ/cm^2 (B) TEM micrograph and size distribution of the final ZnSe/CdS sample after 60 min. The particles have a diameter of 7.8 ± 0.6 nm. The inset shows fringes corresponding to the $\{200\}$ lattice planes of a single particle.

laser at 532 nm close to the $1S_e$-$1S_h$ transition a sharp stimulated emission (SE) band was observed at pump fluences above 4.5 mJ/cm^2 for an optical density of 1.07 (8.4 % transmittance). The peak had a full width at half maximum of 4.8 nm, compared to 25 nm for the steady state PL peak width, and was blue-shifted relative to the PL peak by 2 nm (see inset of Fig. 1A). The shift of the SE peak to higher energies is indicative of a repulsive biexciton binding energy and Stark shift from the spatially separated charge carriers.[9,31–33] No SE was observed for NCs in solution.

The particle diameter was determined to be 7.8 ± 0.6 nm from TEM analysis of the washed particles after 60 min addition. Based on the measured ZnSe core diameter of 3.3 nm diameter, 2.5 nm (8.6 monolayers) of CdS shell material were deposited (Fig. 1B). Signals in the TEM images of single particles that correspond to specific lattice planes were extracted *via* Fourier transformation. The resulting, filtered image allows the core/shell structure of the nanocrystal to be enhanced. The mixture of ZnSe and CdS at the interface breaks the periodicity of the lattice and appears as a gap in the image (see inset of Fig. 1B and supporting information, Fig. S2-3).

Transient Absorption Analysis

In order to better resolve the exciton states that are difficult to observe in steady-state UV/vis spectroscopy, nanosecond transient absorption (TA) spectra were acquired using 355 nm excitation of six ZnSe/CdS samples in hexane, prepared with 3.6 nm cores at shelling temperatures ranging from 260 to 310 °C. All samples showed two clearly separated bleach signals (Fig. 2A) that corresponded closely to the first and second absorption maxima of the nanocrystals and which decayed with approximately the same lifetime as the PL (data not shown). These signals were assigned to the $1S_e$-$1S_h$ and $1S_e$-$2S_h$ exciton states, respectively. Both exciton states are based on the same electron level, which dominates the relaxation kinetics as the more mobile charge carrier.[34,35] Hewa-Kasakarage et al. have assigned similar bleaches in ZnSe/CdS dot-in-a-rod structures to a charge separated state $1S_e$(CdS)-$1S_h$(ZnSe) and to a localized, CdS-based exciton, $1S_e$-$1S_h$.[36] In our spherically symmetrical system, the $1S_e$-$2S_h$ exciton has both charges localized in the shell or in the graded layer, and is therefore equivalent to the CdS-based exciton of the rod system.

The intensity of the two bleach signals was independent of excitation power when observed 10 ns after the excitation pulse. However, the ratio of the signals was observed to be a strong function of the shelling temperature. At low shelling temperatures, (260 °C), the exciton ground state $1S_e$-$1S_h$ bleach was 1.6 times larger than the $1S_e$-$2S_h$ bleach. This ratio decreased with increasing shelling temperature, reaching a ratio close to one at 280-290 °C, and decreasing to a ratio of just 0.6 at 310 °C (see Fig. 2B). Interestingly, a ratio of 1 coincided with the maximum observed PL QY of 50 % and minimum global Stokes shift. The PL lifetime closely follows the trend of the quantum yield until 290 °C and deviates slightly towards longer lifetimes at 300 °C and above (Fig. 3A). This shows that the radiative lifetime of the band edge emission is almost unchanged if the shelling conditions are varied.

Femtosecond transient absorption experiments revealed that the ratio of the bleach signals did not change significantly during the first 750 ps. The bleach intensity is therefore determined by state filling on the sub-picosecond timescale below the timescale of the instrument response function, *i.e.* the differences between the samples are not caused by ultrafast relaxation kinetics from

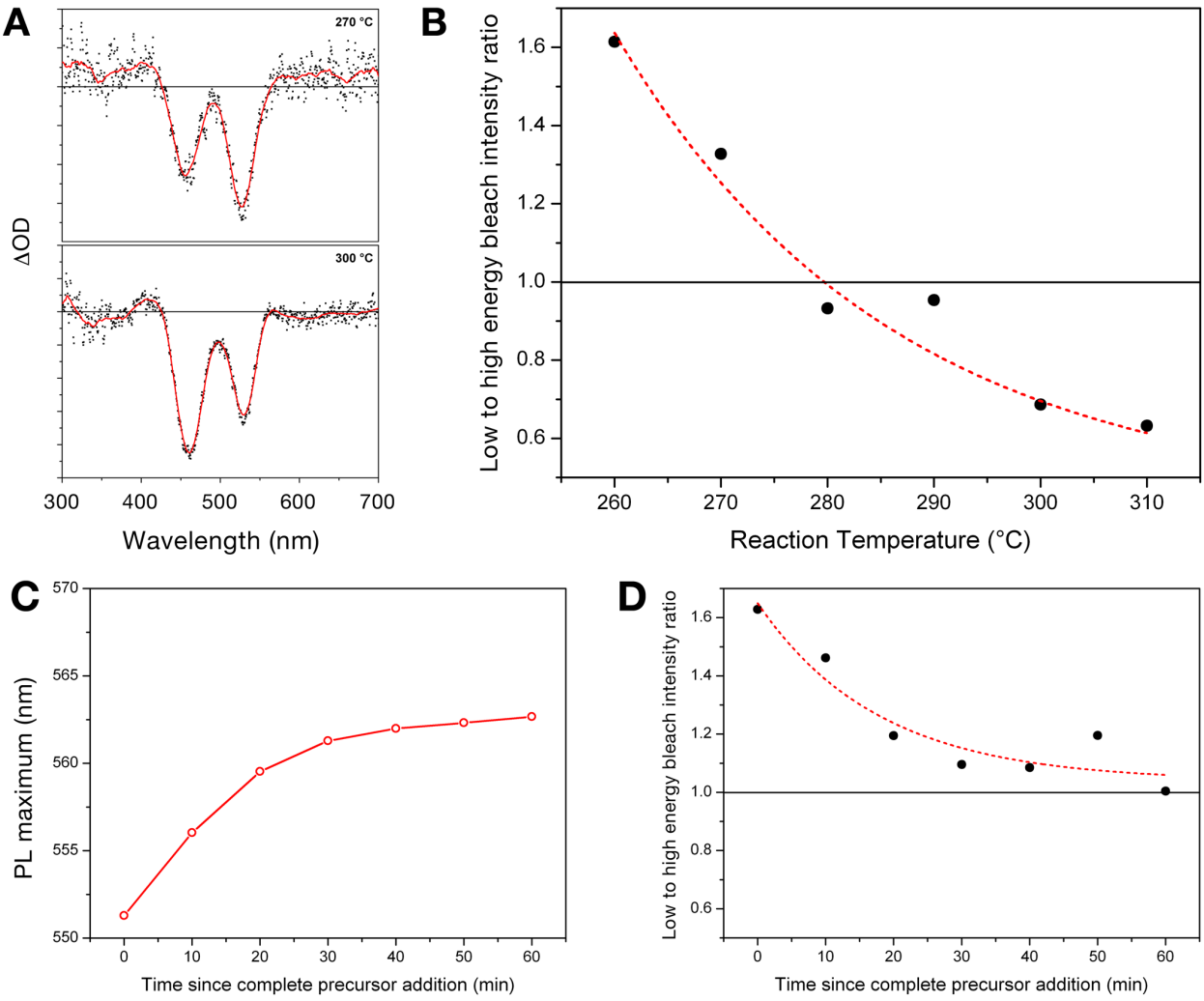


Figure 2: (A) Transient absorption spectra of ZnSe/CdS particles in hexane 10 ns after photoexcitation for 3.6 nm cores and CdS shells grown at 270 °C (top) and 300 °C (bottom). The black dots show the original data, the red curves have been smoothed. (B) The ratio of the integrated peak intensities of the low to high energy bleach signals plotted against reaction temperature. The exponential fit (red dotted line) is a guide to the eye. (C) PL peak positions and (D) integrated peak ratios of the TA spectra for ZnSe/CdS particles grown at 260 °C. The precursors were added over the course of 1 h and allowed to react for 1 h after complete addition.

the 2S to 1S hole state. While the general trend was highly reproducible, the bleach intensity ratios were found to vary slightly with ZnSe core size, with the PL QY maximum occurring at a higher temperature of 300 °C for smaller 3.3 nm cores.

Starting with 3.6 nm core ZnSe particles, it was found that for a constant reaction time of 1 h the final particle diameter increased monotonically with increasing shelling temperature up to 310 °C from 5.4 nm to 7.0 nm with an average standard deviation of 8 % (see supporting information, Fig. S4). While the $1S_e$-$1S_h$ bleach position also exhibited an increasing red-shift up to a shelling temperature of 290 °C, the shift became smaller again at higher temperatures (Fig. 3B). Since the shell thickness increases monotonically up to 310 °C, the exciton peak energy is not controlled simply by overall particle size.

To confirm that the observed shift is not simply due to incomplete shell deposition at lower temperatures, the shell growth was repeated with the same cores at 260 °C, but the colloidal solution was allowed to react for 1 h after complete precursor addition. Fig. 2C-D show that further shell growth occurs until the shift of the PL maximum and bleach intensity ratio both plateau off after approximately 30 minutes. The shift is accompanied by a visible increase in PL intensity. The final NCs are spectroscopically similar to particles grown at 270-280 °C without the additional reaction time. Neither the blue-shifts nor the bleach ratios seen for reactions above 290 °C can be observed. From this we conclude that while higher temperatures accelerate the rate of shell deposition, they also lead to secondary changes in the core-shell structures.

Exciton Oscillator Strength is Governed by Wavefunction Overlap

We explain the changes in bleach intensity ratio, blue-shift of the exciton peaks at higher shelling temperatures, and changes in the PL QY and PL lifetime in terms of increased interfacial alloying between the ZnSe and CdS semiconductors, as proposed in previous work on CdSe/CdS/ZnS.[21] At lower shelling temperatures, thinner shells are deposited, and both PL QY and lifetime are low due to fast non-radiative charge carrier recombination caused by crystal faults at the core/shell interface or particle surface. It has been shown for CdSe/ZnSe particles that up to 270 °C no alloy

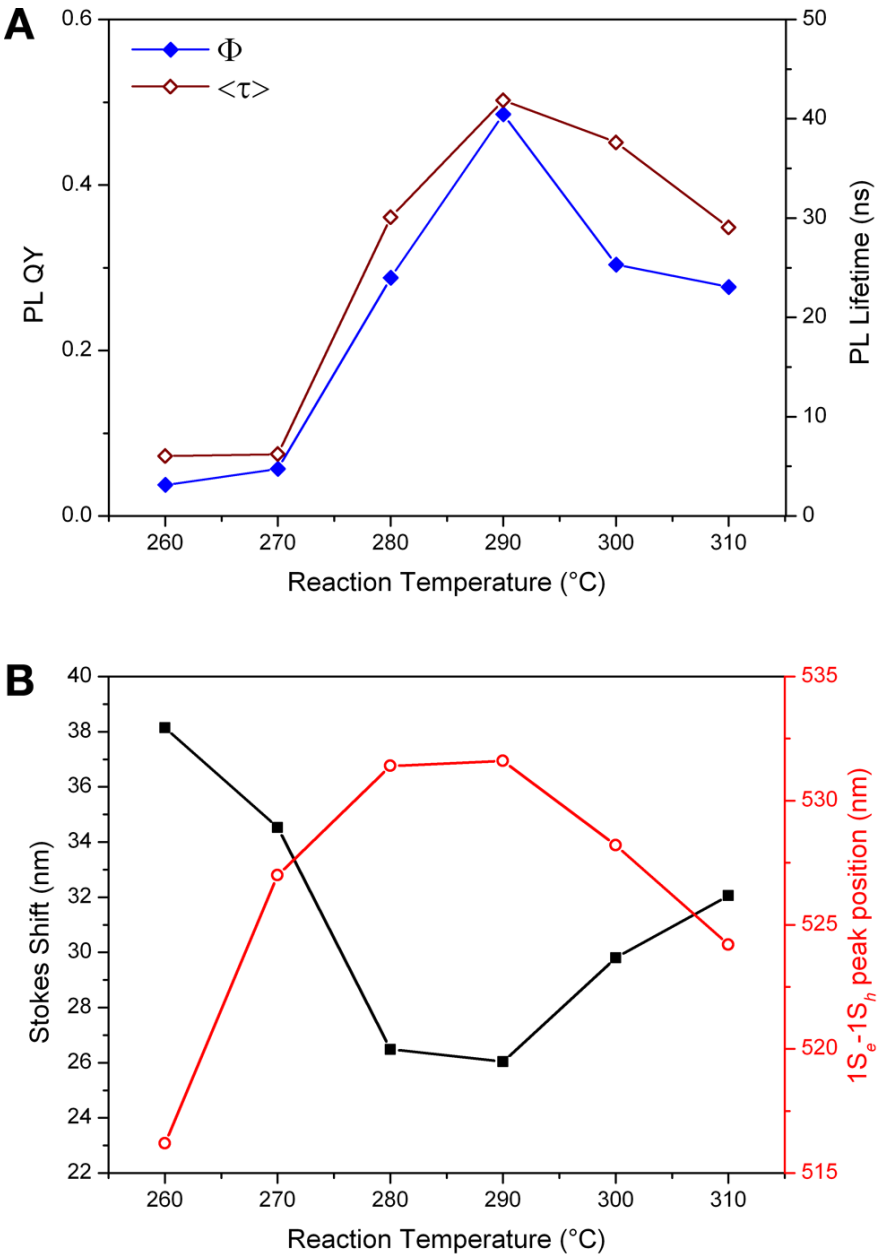


Figure 3: (A) PL quantum yields (Φ, blue) and lifetimes (τ, brown) plotted as a function of shelling temperature. (B) The global Stokes shift (black squares) and the band-edge exciton peak position in Fig. 2 (red open circles) as a function of shelling temperature. Note that the maximum or minimum of each parameter occurs at the same shelling temperature.

formation can be observed,[37] and our data suggest a similar limit for ZnSe/CdS. Above 270 °C, deposited Cd^{2+} ions diffuse into the core ZnSe and a graded interface forms, which closes the fast, non-radiative decay channels and increases the overall PL QY to 50 % and the PL lifetime to $\langle\tau\rangle =$ 42 ns. Additionally, stretched exponential fits of the PL decay yield the largest stretching factor $\beta = 0.71$ (narrowest distribution of lifetimes) for 290 °C (see supporting information, Fig. S8).

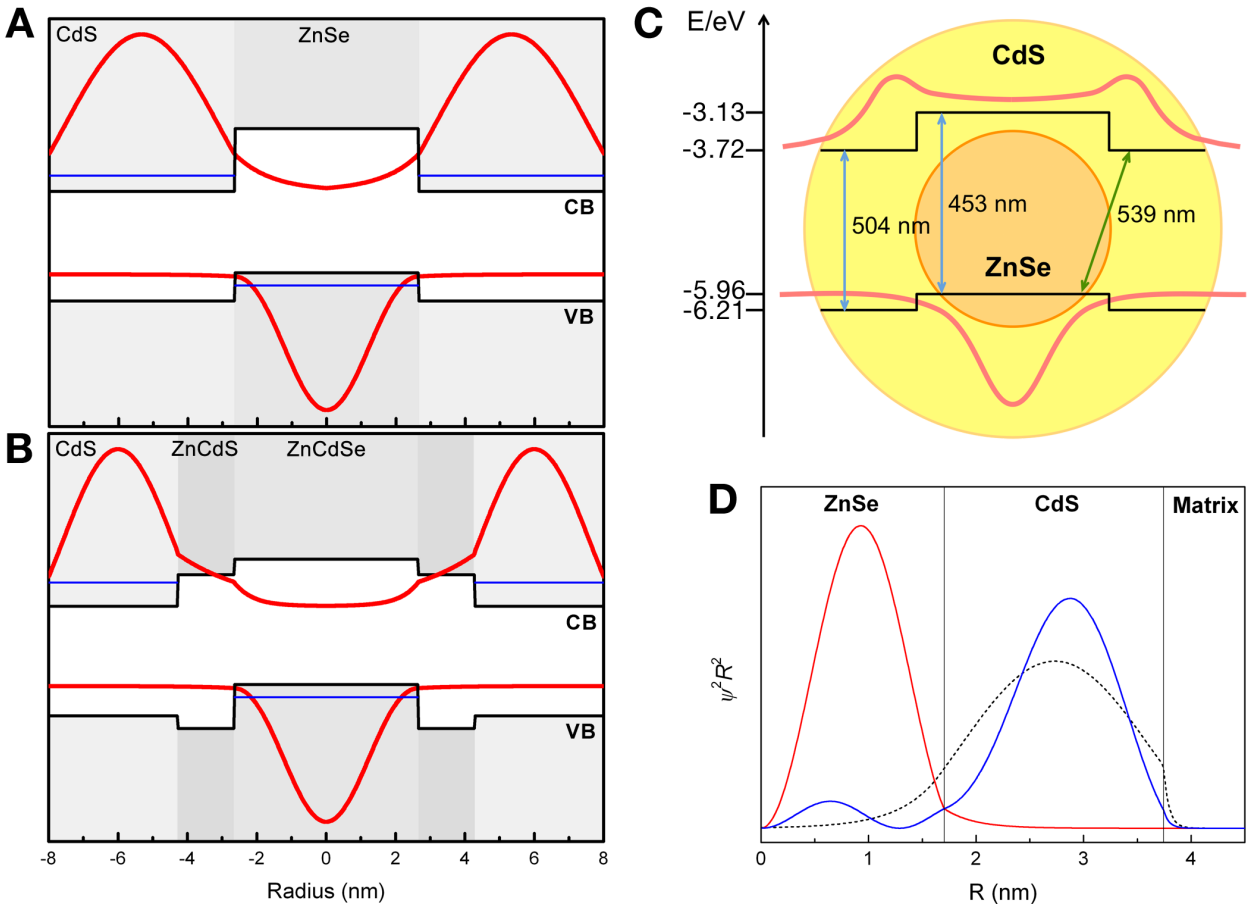


Figure 4: Schematic of the wavefunctions (red), band potentials (black), and lowest energy eigenvalues (blue) in core-shell ZnSe/CdS nanocrystals. (A) shows a single potential step, (B) shows two steps as a first approximation of an alloyed shell. The inner shell consists of ZnSeS, and complete alloying of the core to form ZnCdSe is assumed for simplicity. The alloy causes stronger confinement of the electron in the shell, and at the same time a slower decay of the wavefunction towards the core. (C) Cartoon of a ZnSe/CdS core/shell quantum dot showing wavelengths corresponding to bulk CdS, ZnSe, and spatially indirect band gap transitions. (D) Plots of the radial probability distribution for the first electron state (black, dashed line) and the first (red) and second (blue) hole state reveal a greater overlap of the $1S_e$-$2S_h$ exciton than for the case of the $1S_e$-$1S_h$ exciton.

The body of work on cation exchange reactions for II-VI semiconductor nanoparticles suggests

that alloying at the ZnSe/CdS interface is dominated by cation diffusion, while the anion sublattice is preserved.[38–41] This is confirmed by repeating the shelling at 290 °C in the absence of a sulfur source by just adding an excess of cadmium oleate: The PL spectrum shifts by almost 300 nm from 387 to 675 nm while it undergoes cation exchange from ZnSe to CdSe. The spectrum broadens by a factor of 3.8 at a concentration at which the composition is expected to be ZnCdSe with a 1:1 metal ion ratio, after which it becomes narrower again (see supporting information, Fig. S9). The first absorption maximum shifts in a similar manner, but broadens too much to reliably calculate the peak position.

For thick-shelled particles alloying driven by cation diffusion results in a core with a wide outer region composed of $Zn_xCd_{1-x}Se$ and a comparably thinner region of $Zn_{1-x}Cd_xS$ at the interface. The band gap of alloyed materials lies between those of the pure, constituent compounds.[42] For $Zn_xCd_{1-x}Se$ this lowers the conduction band edge towards that of the shell, while the valence band edge is raised with an increased potential step to the CdS shell. The intermediate $Zn_{1-x}Cd_xS$ layer will further smoothen the conduction band edge gradient, but forms a potential trough in the valence band edge and acts as an additional blocking layer for the hole.

The photophysics in the alloy NCs is a result of two competing effects that occur during alloying:[42] Firstly, the potential step function at the conduction band interface broadens to a potential gradient. Consequently, the charge carriers in low-energy states become more strongly confined by the rise of potential energy in the diffusion zone. This increases the kinetic energy of the charge carrier. Secondly, the exponential decay of the wavefunction into the potential wall becomes more gradual at the interface. This delocalization decreases the kinetic energy of the charge carrier. The effects are illustrated for the electron wavefunction in Fig. 4A-B, in which the gradient is approximated by a two-step function. The apparent blue-shift of the exciton absorption peak at higher temperatures suggests that the confinement term is the dominant contributing factor in the presented data. While the charge carrier overlap of the excited state is increased due to the delocalization, that of the exciton ground state decreases, causing a longer radiative lifetime of the band edge emission, as observed in Fig. 3A. The overall shorter PL lifetimes at shelling temperatures of

300 °C and above are caused by nonradiative relaxation channels. For small particles, thick shells, and high shelling temperatures the core can be completely converted into ZnCdSe, lowering the inter-band gap below the value expected for bulk ZnSe/CdS interfaces of 2.3 eV (absorption at 539 nm, see Fig. 4C).

This conclusion is supported by the change of the bleach intensity ratio, which is a direct measurement of the relative oscillator strengths of the two lowest exciton states. With increasing shelling temperature and shell thickness the electron wavefunction is increasingly confined to the CdS shell, while the 2S hole is shifted towards the graded interface, thus increasing the wavefunction overlap. When the overlap becomes large enough the oscillator strength of the high energy bleach becomes larger than that for the band edge state. Effective mass approximation (EMA) calculations for particles with a 3.6 nm ZnSe core and a 2.0 nm (7 ML) CdS shell give a wavefunction overlap of 0.92 for the $1S_e$-$2S_h$ exciton, compared to 0.28 for the $1S_e$-$1S_h$ ground state (see Fig. 4D).

Growth of an Additional ZnS Shell

The shell synthesis can be extended to enable deposition of a second shell of ZnS onto type-II particles, which acts as a protective layer and isolates the excitons from surface traps. The method works for both the ZnSe/CdS particles discussed above and the inverse type-II configuration CdS/ZnSe, which has been published by Ivanov et al.[11] The PL QY of the latter NCs improves strongly when they are annealed overnight at 160 °C after synthesis, although this causes them to acquire a triangular shape, making determination of a precise shell thickness difficult (see supporting information, Fig. S5).

As previously described for CdSe/CdS/ZnS,[21] the optimal temperature for ZnS growth lies below that for CdS. At 270 °C the additional ZnS shell increased the PL QY of ZnSe/CdS NCs from 27 to 75 %, and of CdS/ZnSe NCs from 9 to 41 %. While CdS/ZnSe particles degraded at reaction temperatures of 280 °C and above (see supporting information, Fig. S6), ZnSe/CdS/ZnS particles were successfully made at 310 °C, albeit with a significantly decreased PL QY (4 %).

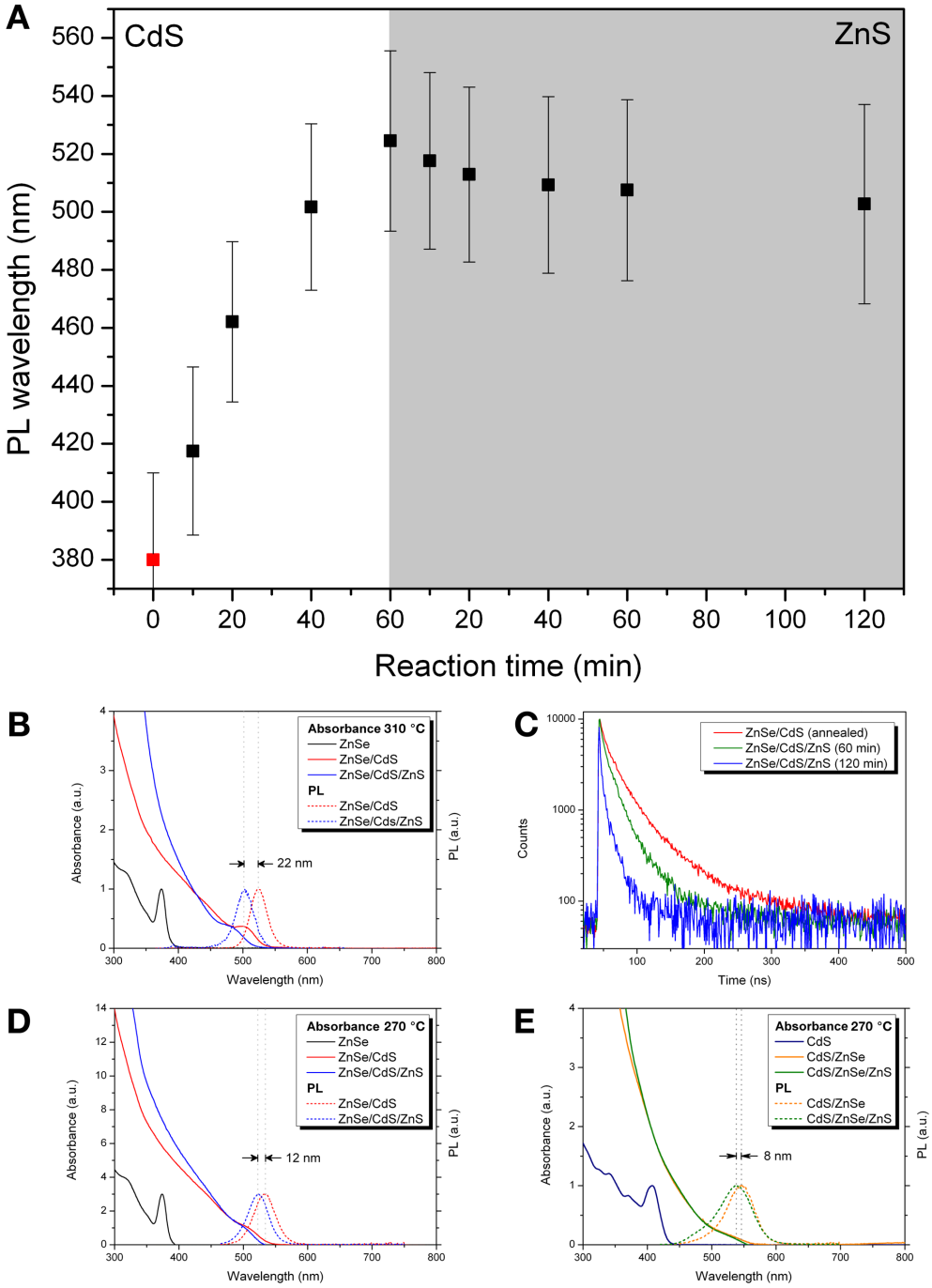


Figure 5: (A) Shift of the PL maximum during successive growth of CdS (white background) and ZnS (grey background) onto ZnSe particles of 3.3 nm diameter at 310°C. The reaction time is reset to 0 at the beginning of ZnS deposition. (B) Normalized absorption and PL spectra of the above particles. Spectra of the cores (black) and completed core/shell and core/shell/shell particles are shown. (C) PL decay curves of the above particles during ZnS growth. (D) Absorption and PL spectra of the same reaction performed at 270°C. (E) Absorption and PL spectra of CdS, CdS/ZnSe, and CdS/ZnSe/ZnS particles with the ZnS shell grown at 270°C.

ZnSe/CdS/ZnS particles appear spherical and monodisperse (see supporting information, Fig. S7) and exhibit comparable TA spectra to the ZnSe/CdS particles described above (see supporting information, Fig. S10). During ZnS deposition the PL spectrum blue-shifts by 21.8 nm, which amounts to a 15 % reversal of the red-shift induced by the growth of the CdS shell. During the blue-shift a sharp decrease of the PL lifetime from $\langle\tau\rangle = 27.5$ ns down to $\langle\tau\rangle = 15.6$ ns after 60 min and $\langle\tau\rangle = 3.9$ ns after 120 min was observed at 310 °C (Fig. 5A-C). This confirms that our postulated alloying model[21] applies to a wide range of II-VI semiconductors. Diffusion of ions between the shell materials causes the formation of a gradual increase of the band potential well within the inner shell. The electron wavefunction is thus more strongly confined to the inner particle. While for long reaction times the decreased lifetime can be attributed to new, non-radiative relaxation channels that cause the drop in PL QY, it is likely that an increased overlap of electron and hole contributes to the faster relaxation, pushing the electronic structure back towards the *quasi*-type-II regime. In accordance with the conclusions for ZnSe/CdS the ion diffusion is reduced at 270 °C, causing a smaller blue-shift of 12 nm for ZnSe/CdS/ZnS, and 8 nm for CdS/ZnSe/ZnS (Fig. 5D-E).

CONCLUSIONS

In summary, we have shown a simple and versatile route to highly emissive ZnSe/CdS Type-II core/shell quantum dots that extends high temperature, alkanethiol-based shell deposition synthesis from CdSe/CdS/ZnS to other II-VI semiconductors. Based on spectroscopic observations, there is extensive, temperature-dependent interfacial alloying between the core and shell materials. Alloying can be used to tune the electronic structure of Type-II particles by controlling the charge carrier overlap in the interfacial diffusion layer. Shelling temperature, precursor addition rate, initial core particle size, and final shell thickness all determine the final electronic band structure and photo physical properties of the resultant core-shell nanocrystals. A reaction temperature of 290-300 °C yields the highest PL QYs and smallest Stokes shifts for 3.7 nm cores. The particles show stimulated emission at room temperature in closely packed samples for low pump fluences

of 4.5 mJ/cm^2 and above. An additional layer of ZnS can be grown on both ZnSe/CdS and the inverse structure CdS/ZnSe in order to significantly improve the luminescence efficiency.

Associated Content

Supporting Information Available

TEM analysis, UV/vis spectra and PL decay curves for different shelling temperatures, TA spectra for ZnSe/CdS/ZnS particles. This material is available free of charge via the Internet at `http://pubs.acs.org/`.

Author Information

Author Contributions

K.B. performed nanocrystal synthesis, performed spectroscopic analysis and wrote the manuscript. K.N.S. and T.A.S. performed and analyzed femtosecond TA spectroscopy and measured amplified stimulated emission. N.K. contributed to the development of ZnS shell deposition and nanosecond TA spectroscopy. All authors have given approval to the final version of the manuscript.

Notes

The authors declare no competing financial interests.

Acknowledgements

The authors thank Dr. Jacek Jasieniak and Prof. Kenneth P. Ghiggino for helpful discussions. K.B. acknowledges the support of the Alexander von Humboldt Foundation through a Feodor Lynen research fellowship. K.N.S acknowledges scholarship and funding support of the Australian

Government through the Australian Renewable Energy Agency (ARENA). Responsibility for the views, information or advice expressed herein is not accepted by the Australian Government. N.K. thanks the Melbourne Materials Institute for support through an MMI/CSIRO scholarship. T.A.S. acknowledges support from the ARC Centre of Excellence for Coherent X-Ray Science. P.M. acknowledges the support of the ARC through DP 130102134.

References

(1) Talapin, D. V.; Rogach, A. L.; Kornowski, A.; Haase, M.; Weller, H. Highly Luminescent Monodisperse CdSe and CdSe/ZnS Nanocrystals Synthesized in a Hexadecylamine-Trioctylphosphine Oxide-Trioctylphospine Mixture. *Nano Lett.* **2001**, *1*, 207–211.

(2) Manna, L.; Scher, E. C.; Li, L.; Alivisatos, A. P. Epitaxial Growth and Photochemical Annealing of Graded CdS/ZnS Shells on Colloidal CdSe Nanorods. *J. Am. Chem. Soc.* **2002**, *124*, 7136–7145.

(3) Talapin, D. V.; Mekis, I.; Götzinger, S.; Kornowski, A.; Benson, O.; Weller, H. CdSe/CdS/ZnS and CdSe/ZnSe/ZnS Core-Shell-Shell Nanocrystals. *J. Phys. Chem. B* **2004**, *108*, 18826–18831.

(4) van Embden, J.; Jasieniak, J. J.; Gómez, D. E.; Mulvaney, P.; Giersig, M. Review of the Synthetic Chemistry Involved in the Production of Core/Shell Semiconductor Nanocrystals. *Aust. J. Chem.* **2007**, *60*, 457–471.

(5) Donegá, C. d. M. Synthesis and Properties of Colloidal Heteronanocrystals. *Chem. Soc. Rev.* **2011**, *40*, 1512.

(6) Greytak, A. B.; Allen, P. M.; Liu, W.; Zhao, J.; Young, E. R.; Popović, Z.; Walker, B. J.; Nocera, D. G.; Bawendi, M. G. Alternating Layer Addition Approach to CdSe/CdS Core/Shell Quantum Dots with Near-Unity Quantum Yield and High On-Time Fractions. *Chem. Sci.* **2012**, *3*, 2028.

(7) Balet, L. P.; Ivanov, S. A.; Piryatinski, A.; Achermann, M.; Klimov, V. I. Inverted Core/Shell Nanocrystals Continuously Tunable between Type-I and Type-II Localization Regimes. *Nano Lett.* **2005**, *4*, 1485–1488.

(8) Chin, P. T. K.; de Mello Donegá, C.; van Bavel, S. S.; Meskers, S. C. J.; Sommerdijk, N. A. J. M.; Janssen, R. A. J. Highly Luminescent CdTe/CdSe Colloidal Heteronanocrystals with Temperature-Dependent Emission Color. *J. Am. Chem. Soc.* **2007**, *129*, 14880–14886.

(9) Klimov, V. I.; Ivanov, S. A.; Nanda, J.; Achermann, M.; Bezel, I. V.; Mcguire, J. A.; Piryatinski, A. Single-Exciton Optical Gain in Semiconductor Nanocrystals. *Nature* **2007**, *447*, 441–446.

(10) Ivanov, S. A.; Nanda, J.; Piryatinski, A.; Achermann, M.; Balet, L. P.; Bezel, I. V.; Anikeeva, P. O.; Tretiak, S.; Klimov, V. I. Light Amplification Using Inverted Core/Shell Nanocrystals: Towards Lasing in the Single-Exciton Regime. *J. Phys. Chem. B* **2005**, *108*, 10625–10630.

(11) Ivanov, S. A.; Piryatinski, A.; Nanda, J.; Tretiak, S.; Zavadil, K. R.; Wallace, W. O.; Werder, D.; Klimov, V. I. Type-II Core/Shell CdS/ZnSe Nanocrystals: Synthesis, Electronic Structures, and Spectroscopic Properties. *J. Am. Chem. Soc.* **2007**, *129*, 11708–11719.

(12) Dorfs, D.; Salant, A.; Popov, I.; Banin, U. ZnSe Quantum Dots Within CdS Nanorods: A Seeded-Growth Type-II System. *Small* **2008**, *4*, 1319–1323.

(13) Zhang, W.; Chen, G.; Wang, J.; Ye, B.-C.; Zhong, X. Design and Synthesis of Highly Luminescent Near-Infrared-Emitting Water-Soluble CdTe/CdSe/ZnS Core/Shell/Shell Quantum Dots. *Inorg. Chem.* **2009**, *48*, 9723–9731.

(14) Wei, S.-H.; Zunger, A. Calculated Natural Band Offsets of all II–VI and III–V Semiconductors: Chemical Trends and the Role of Cation *d* Orbitals. *Appl. Phys. Lett.* **1998**, *72*, 2011.

(15) Karazhanov, S.; Lew Yan Voon, L. Ab initio Studies of the Band Parameters of III–V and II–VI Zinc-Blende Semiconductors. *Semiconductors* **2005**, *39*, 161–173.

(16) Steiner, D.; Dorfs, D.; Banin, U.; della Sala, F.; Manna, L.; Millo, O. Determination of Band Offsets in Heterostructured Colloidal Nanorods Using Scanning Tunneling Spectroscopy. *Nano Lett.* **2008**, *8*, 2954–2958.

(17) van de Walle, C. G.; Neugebauer, J. Universal Alignment of Hydrogen Levels in Semiconductors, Insulators and Solutions. *Nature* **2003**, *423*, 626–628.

(18) Nethercot Jr, A. Prediction of Fermi Energies and Photoelectric Thresholds Based on Electronegativity Concepts. *Phys. Rev. Lett.* **1974**, *33*, 1088–1091.

(19) Dorfs, D.; Franzl, T.; Osovsky, R.; Brumer, M.; Lifshitz, E.; Klar, T. A.; Eychmüller, A. Type-I and Type-II Nanoscale Heterostructures Based on CdTe Nanocrystals: A Comparative Study. *Small* **2008**, *4*, 1148–1152.

(20) Chen, O. et al. Compact High-Quality CdSe-CdS Core-Shell Nanocrystals with Narrow Emission Linewidths and Suppressed Blinking. *Nat. Mater.* **2013**, *12*, 445–451.

(21) Boldt, K.; Kirkwood, N.; Beane, G. A.; Mulvaney, P. Synthesis of Highly Luminescent and Photo-Stable, Graded Shell CdSe/$Cd_xZn_{1-x}S$ Nanoparticles by *In Situ* Alloying. *Chem. Mater.* **2013**, *25*, 4731–4738.

(22) Park, Y.-S.; Bae, W. K.; Padilha, L.; Pietryga, J. M.; Klimov, V. I. Effect of the Core/Shell Interface on Auger Recombination Evaluated by Single-Quantum-Dot Spectroscopy. *Nano Lett.* **2014**, 140107104206002.

(23) Kaniyankandy, S.; Rawalekar, S.; Ghosh, H. N. Charge Carrier Cascade in Type II CdSe–CdTe Graded Core–Shell Interface. *J. Mater. Chem. C* **2013**, *1*, 2755.

(24) Cozzoli, P. D.; Manna, L.; Curri, M. L.; Kudera, S.; Giannini, C.; Striccoli, M.; Agostiano, A.

Shape and Phase Control of Colloidal ZnSe Nanocrystals. *Chem. Mater.* **2005**, *17*, 1296–1306.

(25) Cao, Y. C.; Wang, J. One-Pot Synthesis of High-Quality Zinc-Blende CdS Nanocrystals. *J. Am. Chem. Soc.* **2004**, *126*, 14336–14337.

(26) Yu, W. W.; Qu, L.; Guo, W.; Peng, X. Experimental Determination of the Extinction Coefficient of CdTe, CdSe, and CdS Nanocrystals. *Chem. Mater.* **2005**, *15*, 2854–2860.

(27) Schlegel, G.; Bohnenberger, J.; Potapova, I.; Mews, A. Fluorescence Decay Time of Single Semiconductor Nanocrystals. *Phys. Rev. Lett.* **2002**, *88*, 137401.

(28) Sugunan, S. K.; Robotham, B.; Sloan, R. P.; Szmytkowski, J.; Ghiggino, K. P.; Paige, M. F.; Steer, R. P. Photophysics of Untethered ZnTPP-Fullerene Complexes in Solution. *J. Phys. Chem. A* **2011**, *115*, 12217–12227.

(29) van Embden, J.; Jasieniak, J. J.; Mulvaney, P. Mapping the Optical Properties of CdSe/CdS Heterostructure Nanocrystals: The Effects of Core Size and Shell Thickness. *J. Am. Chem. Soc.* **2009**, *131*, 14299–14309.

(30) Chen, Y.; Vela, J.; Htoon, H.; Casson, J. L.; Werder, D. J.; Bussian, D. A.; Klimov, V. I.; Hollingsworth, J. A. "Giant" Multishell CdSe Nanocrystal Quantum Dots with Suppressed Blinking. *J. Am. Chem. Soc.* **2008**, *130*, 5026–5027.

(31) Klimov, V. I.; Mikhailovsky, A. A.; Xu, S.; Malko, A.; Hollingsworth, J. A.; Leatherdale, C. A.; Eisler, H.; Bawendi, M. G. Optical Gain and Stimulated Emission in Nanocrystal Quantum Dots. *Science* **2000**, *290*, 314–317.

(32) Bansal, B.; Godefroo, S.; Hayne, M.; Medeiros-Ribeiro, G.; Moshchalkov, V. Extended Excitons and Compact Heliumlike Biexcitons in Type-II Quantum Dots. *Phys. Rev. B* **2009**, *80*, 205317.

(33) Oron, D.; Kazes, M.; Banin, U. Multiexcitons in type-II Colloidal Semiconductor Quantum Dots. *Phys. Rev. B* **2007**, *75*, 35330.

(34) Yan, Y.; Chen, G.; Van Patten, P. G. Ultrafast Exciton Dynamics in CdTe Nanocrystals and Core/Shell CdTe/CdS Nanocrystals. *J. Phys. Chem. C* **2011**, *115*, 22717–22728.

(35) Kambhampati, P. Unraveling the Structure and Dynamics of Excitons in Semiconductor Quantum Dots. *Acc. Chem. Res.* **2011**, *44*, 1–13.

(36) Hewa-Kasakarage, N. N.; Kirsanova, M.; Nemchinov, A.; Schmall, N.; El-Khoury, P. Z.; Tarnovsky, A. N.; Zamkov, M. Radiative Recombination of Spatially Extended Excitons in (ZnSe/CdS)/CdS Heterostructured Nanorods. *J. Am. Chem. Soc.* **2009**, *131*, 1328–1334.

(37) Zhong, X.; Han, M.; Dong, Z.; White, T. J.; Knoll, W. Composition-Tunable $Zn_xCd_{1-x}Se$ Nanocrystals with High Luminescence and Stability. *J. Am. Chem. Soc.* **2003**, *125*, 8589–8594.

(38) Robinson, R. D.; Sadtler, B.; Demchenko, D. O.; Erdonmez, C. K.; Wang, L. W.; Alivisatos, A. P. Spontaneous Superlattice Formation in Nanorods Through Partial Cation Exchange. *Science* **2007**, *317*, 355–358.

(39) Jain, P. K.; Amirav, L.; Aloni, S.; Alivisatos, A. P. Nanoheterostructure Cation Exchange: Anionic Framework Conservation. *J. Am. Chem. Soc.* **2010**, *132*, 9997–9999.

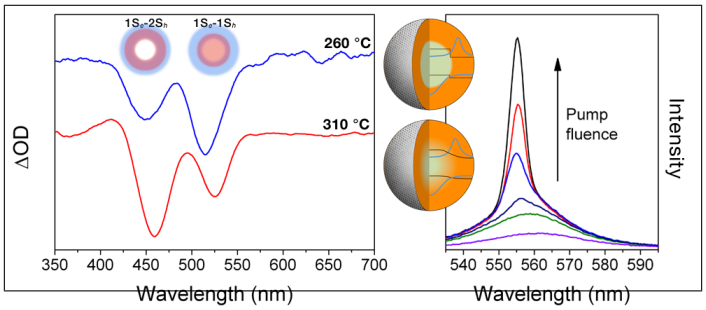
(40) Li, H. et al. Blue-UV-Emitting ZnSe(Dot)/ZnS(Rod) Core/Shell Nanocrystals Prepared from CdSe/CdS Nanocrystals by Sequential Cation Exchange. *ACS Nano* **2012**, *6*, 1637–1647.

(41) Groeneveld, E.; Witteman, L.; Lefferts, M.; Ke, X.; Bals, S.; Van Tendeloo, G.; de Mello Donegá, C. Tailoring ZnSe–CdSe Colloidal Quantum Dots *via* Cation Exchange: From Core/Shell to Alloy Nanocrystals. *ACS Nano* **2013**, *7*, 7913–7930.

(42) Wei, H.; Ren, X.; Han, Z.; Li, T.; Su, Y.; Wei, L.; Cong, F.; Zhang, Y. Facile One-Pot

Synthesis and Band Gap Calculations of $Zn_xCd_{1-x}S$ Nanorods. *Materials Letters* **2013**, *102-103*, 94–97.

Graphical TOC Entry



For Table of Contents Only